MARS and G4beamline simulations of AP2 beamline

V. Tishchenko* and W.M. Morse

Brookhaven National Laboratory, Upton, NY 11973, USA

J.-F. Ostiguy, J. Morgan, and D. Still

Fermi National Accelerator Laboratory, Batavia, IL 60510, USA

M.J. Syphers

Michigan State University, East Lansing, MI 48824, USA

(muon (g-2) collaboration)

(Dated: May 6, 2014)

Abstract

`MARS` and `G4beamline` codes were used to simulate pion production in a target, focusing of the secondary beam by the Lithium lens, collection of muons from pion decay and beam transport through the current AP2 beamline. Muon-to-pion ratio at the end of the AP2 beam line was found to be about 13%. The results of these simulations can be used for benchmarking the simulation code against test-beam measurements at Fermilab.

I. INTRODUCTION

The number of stored muons per proton on target (POT) is a very important quantity for the muon $(g-2)$ experiment E989 at Fermilab. It drives the design of the experiment (beam monitors, positron calorimeters, etc.) and determines the running time which will be needed to accumulate the required statistics. So far, the estimates of this quantity have been based on simulations (`MARS`, `G4beamline` and `phase-space` approach). Resent measurements with test beam at Fermilab [1] opened up a unique opportunity to benchmark our simulations against experimental data. The goal of this note is to simulate pion production in the target, pion and muon collection and transport through the AP2 beam line. The number of muons per POT and muon-to-pion ratio at the end of the AP2 beamline can be directly compared to the quantities measured in the test beam experiment.

* vtishchenko@bnl.gov; https://pubweb.bnl.gov/~vtishchenko

II. MARS MODEL

Pion production in the target and focusing of the pion beam by the Lithium lens were simulated using MARS. The MARS model of the production target and Lithium lens originally provided to us by S. Striganov. A slightly modified version of the MARS model was used in our previous studies[2]. For completeness, we reproduce it again in Fig. 1. The primary proton beam with kinetic energy of 8 GeV impinges on the pion production target (1), which is a vertical 12.7-cm-diameter cylinder with a chord along the proton beam axis of about 7.5 cm in the inconel layer. A secondary beam of charged particles produced in the target is focused by the 16-cm-long 2-cm-diameter Li-lens with 232 T/m magnetic field gradient. Charged particles (π^+ and μ^+) entering a virtual detector (3) installed at the downstream face of the Li-lens are dumped into a file on disk for further tracking in G4beamline.

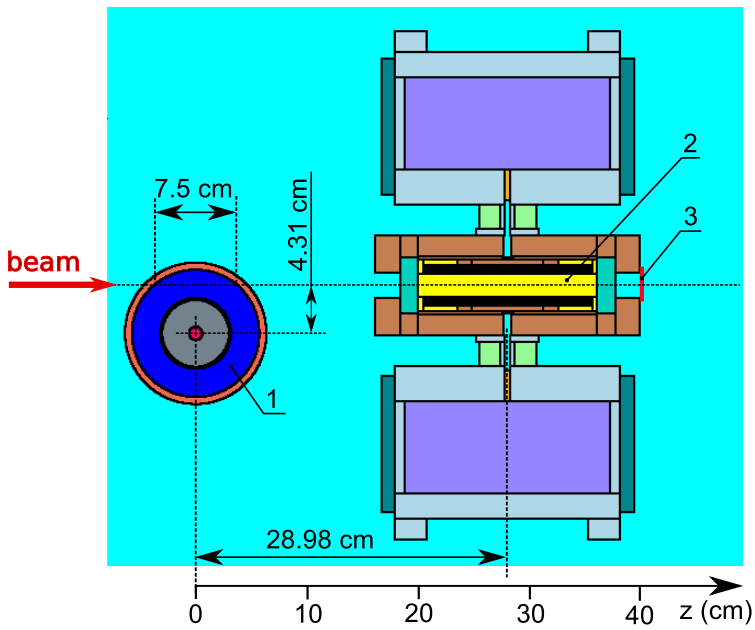

FIG. 1: MARS model of the E989 target station (top view): inconel target (1), 16-cm-long 2-cm-diameter Li cylinder with magnetic field (2), virtual detector, $z = 40.9$ cm (3).

The primary proton beam starts 5 cm upstream from the target and has Gaussian spatial and angular distribution. The parameters of the distributions are adjusted such that in the absence of the target the beam is focused at $z = 0$ to form a spot with $\sigma_x = \sigma_y = 1$-mm and $\sigma_{x'} = \sigma_{y'} = 0.3$-mrad. The parameters of the setup are summarized in Table 1.

TABLE I: Some parameters used in the MARS model of the production target and Li-lens.

name	value
proton beam kinetic energy	8 GeV
Beam spot size (Gaussian shape)	$\sigma_x = \sigma_y = 1$ mm at $z = 0$
Angular spread of the beam	$\sigma_{x'} = \sigma_{y'} = 0.3$ mrad
Distance between Li-lens and target (center-to-center)	28.98 cm
Focusing field gradient of Li-lens	232 T/m

TABLE II: Apertures of AP2 magnets

magnet name	comment
SDEW (VIKIK)	79 mm tall by 127 mm wide rectangle
LQE	159 mm diameter circle
LQB	159 mm diameter circle
LQC	159 mm diameter circle
VISEP	39 mm wide by 53 mm tall[1)]
SDFW	98 mm tall by 127 mm wide rectangle
H704	134 mm wide by 54 mm tall rectangle (MDC magnet)
PMAG	51 mm wide by 35 tall
V730	127 mm tall by 79 mm wide rectangle (CDC magnet)
SQC	Star chamber, see [3]
SQB	Star chamber, see [3]
SQA	Star chamber, see [3]
SQE	Star chamber, see [3]
SQD	Star chamber, see [3]

[1)] Opening for a circulating beam was not modeled

III. G4BEAMLINE MODEL

G4beamline model of the AP2 beamline is shown in Fig. 2. The list of magnet apertures is given in Table II.

To record the beam particles for the offline analysis we installed several virtual detectors, a START detector at the downstream face of the Li-lens; a STOP detector at the downstream face of the last magnet; one detector before the bend (VD_H717, at the upstream face of the dipole magnet H717) and one detector after the bend (VD_Q722, at the upstream face of quadrupole Q722). The location of virtual detectors is indicated in Fig. 2.

The Fermilab Test-Beam Team requested the information on beam rates at several locations in the AP2 beamline for comparison with experimental data. Therefore we added the following virtual detectors, VD_Q_703_704 between quadrupoles Q703 and Q704; VD_Q_705_706 between quadrupoles Q705 and Q706; VD_Q_709_710 between quadrupoles Q709 and Q710; VD_Q_714_716 between quadrupoles Q714 and Q715; VD_Q_727_728 between quadrupoles Q727 and Q728. The location of these detectors is indicated in Fig. 3.

IV. SIMULATIONS

The simulations were conducted at the RACF computing farm at BNL [4]. 3×10^9 protons on target was simulated in MARS. Beam particles (π^+, μ^+, e^+, p) at the downstream face of Li-lens (kinetic energy threshold 1.7 GeV, momentum cutoff 8 GeV/c)were dumped into a data file for tracking in G4beamline. Two data sets were produced using G4beamline, *i*) simulations with all stochastic processes and decay of unstable particles disabled to study beam transmission through the AP2 beamline and *ii*) ordinary data set using QGSP_BERT physics list.

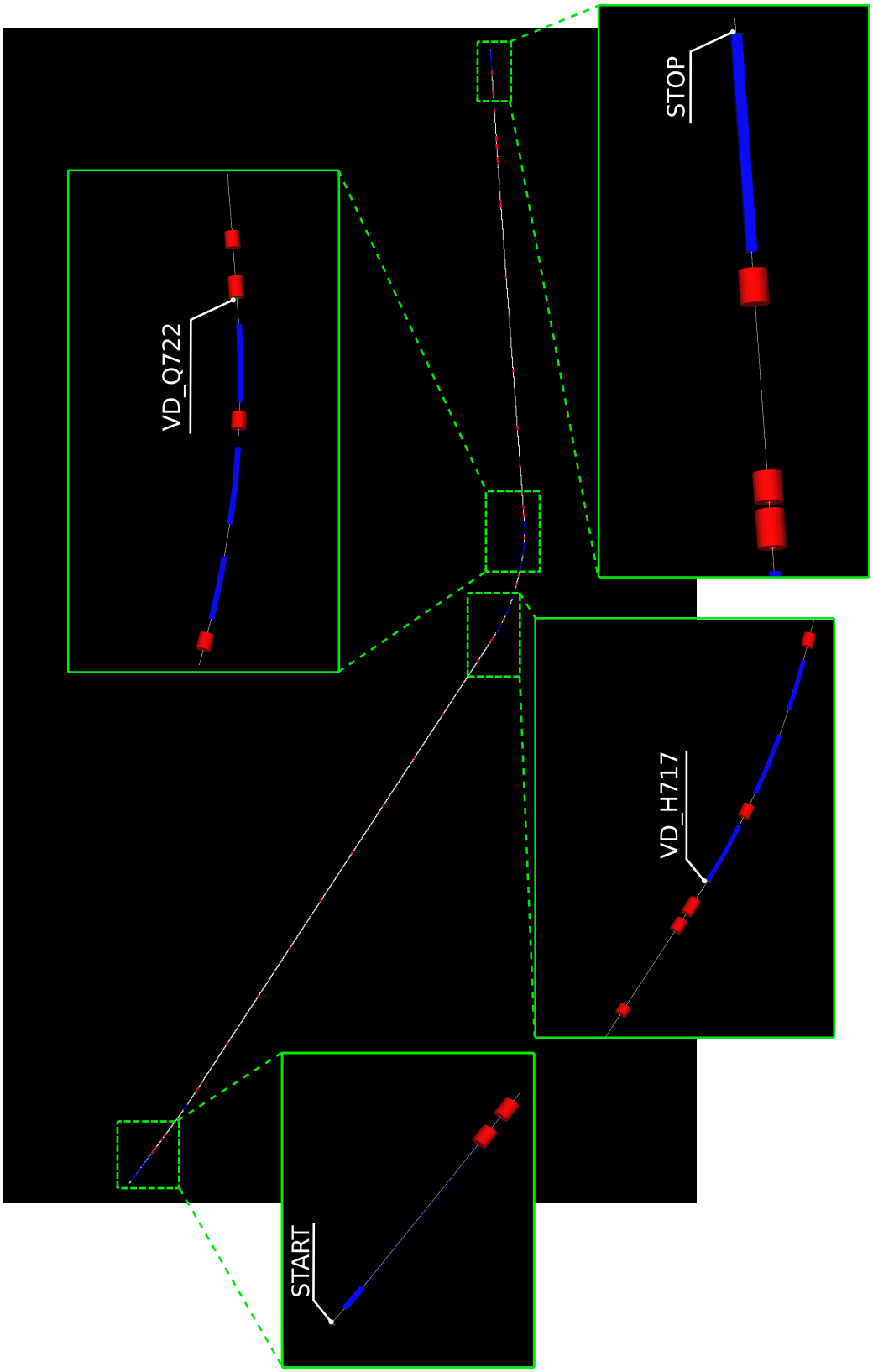

FIG. 2: `G4beamline` model of the AP2 beamline. Red are quadrupole magnets, blue are dipole magnets. The locations of virtual detectors `START`, `VD_H717`, `VD_Q722` and `STOP` are indicated in the inserts which show magnified views of correspoing beamline fragments.

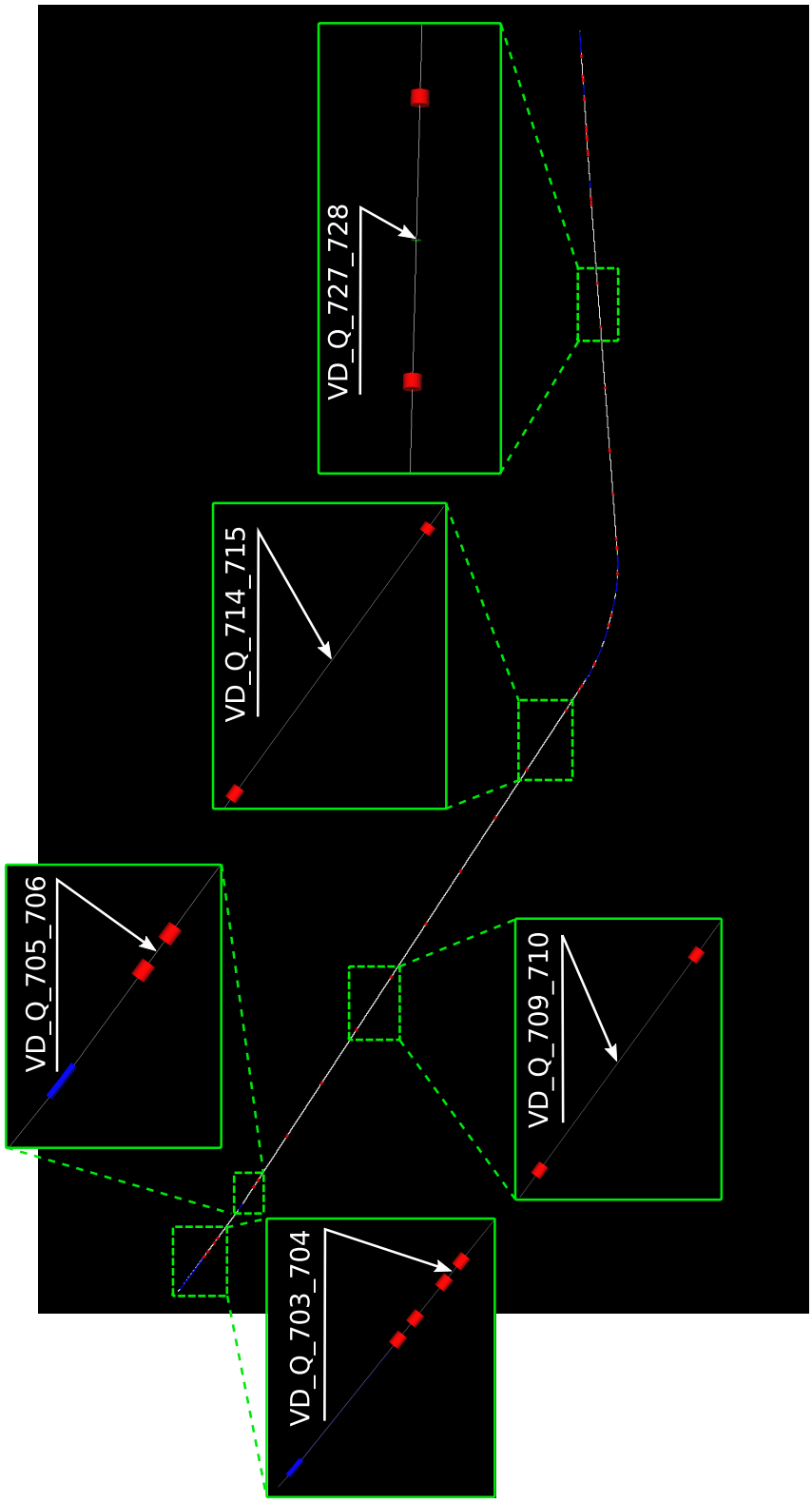

FIG. 3: `G4beamline` model of the AP2 beamline. Red are quadrupole magnets, blue are dipole magnets. The locations of virtual detectors `VD_Q_703_704`, `VD_Q_705_706`, `VD_Q_709_710`, `VD_Q_714_716`, `VD_Q_727_728` are indicated in the inserts which show magnified views of correspoing beamline fragments.

V. BEAM TRANSMISSION

To study the transmission of the beam through the AP2 beamline we disabled all stochastic processes in `G4beamline` including decays of unstable particles. Phase space distributions of all or transmitted particles in the `START` detector are shown in Fig. 4.

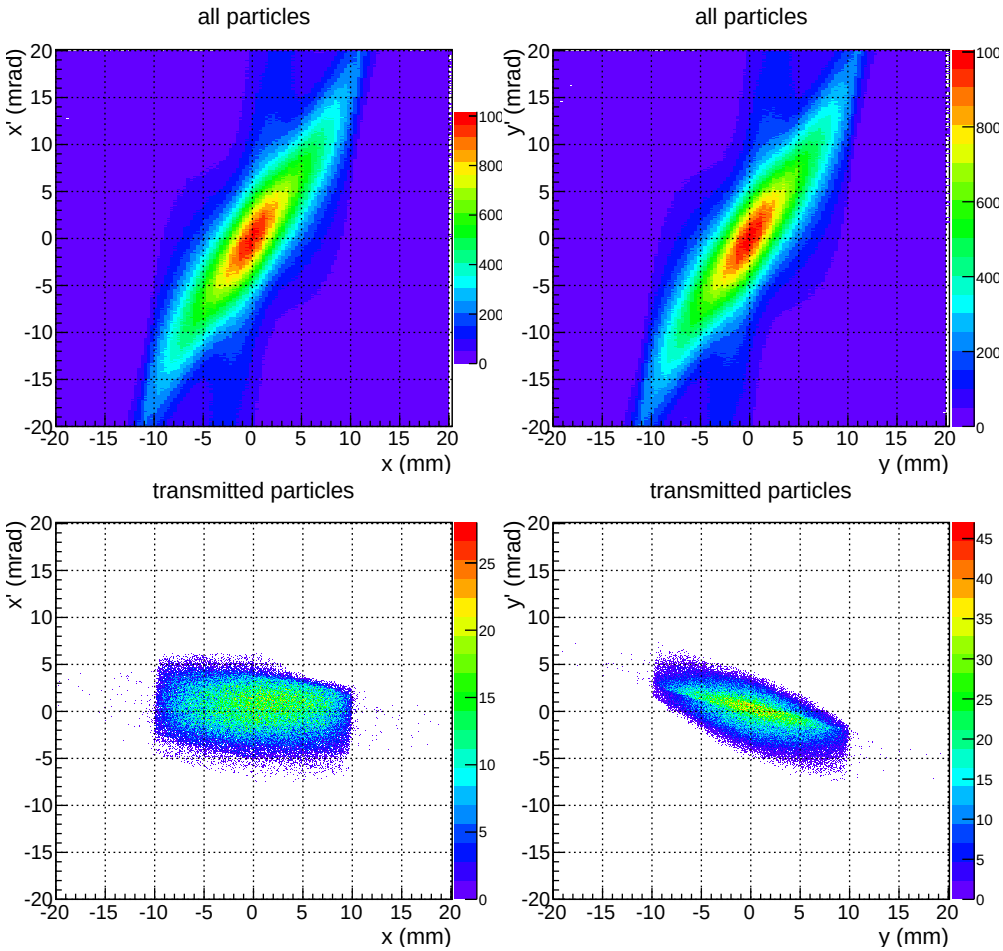

FIG. 4: Horizontal (x-x') and vertical (y-y') phase space distributions of particles in the `START` detector, all particles (top row) or transmitted particles (bottom row). Decay of unstable particles was disabled in `G4beamline`.

The momentum distribution of pions in virtual detectors is shown in Fig. 5. Table III summarizes counting rates and widths of momentum distributions.

VI. MUON COLLECTION AND TRANSMISSION

For studies in this section we enable stochastic processes in `G4beamline` including decays of unstable particles. The momentum distributions of pions and muons in virtual detectors is shown in Fig. 6. Counting rates are summarized in Table IV.

Thus, muon to pion ratio at the end of AP2 beam line is about 13%.

Phase space distributions of beam particles, x-y correlations of hits in virtual detectors and momentum distributions are summarized in Figs. 7-15.

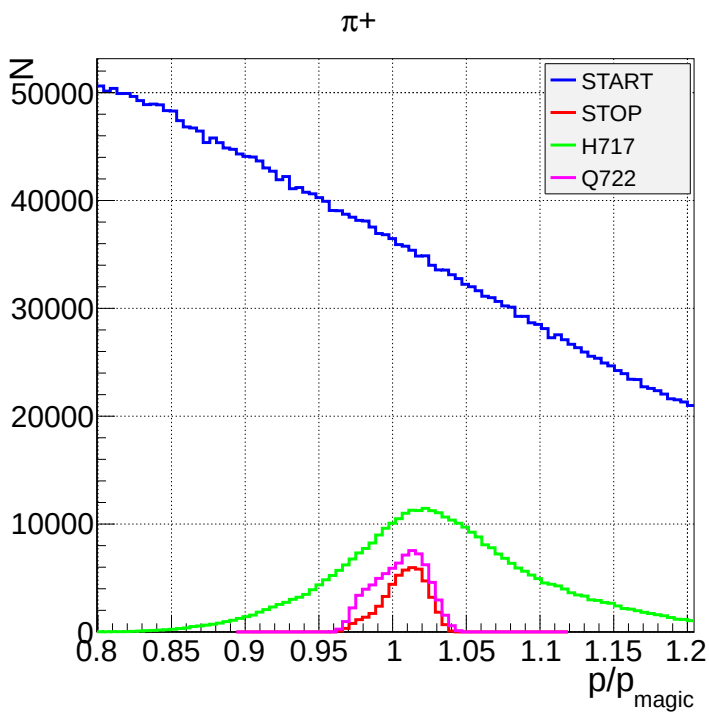

FIG. 5: Momentum distribution of pions in virtual detectors as indicated in the insert. Pion decay disabled.

TABLE III: Counting rates N_x of beam particles in various detectors per 3×10^9 POT and widths of momentum distributions deduced from Gaussian fit to the data. Decay of unstable particles disabled.

Detector	N_{π^+}	N_{μ^+}	N_{e^+}	N_p	$\sigma_p/p_{\rm magic}$ (%)
START	6.38×10^6	1.16×10^4	1.10×10^5	3.96×10^7	*)
VD_Q_703_704	9.85×10^5	1.23×10^3	1.23×10^4	1.82×10^6	13.0
VD_H717	3.83×10^5	337	3.45×10^3	6.97×10^5	6.0
VD_Q722	7.57×10^4	72	706	1.14×10^5	1.9
STOP	4.89×10^4	44	442	7.39×10^4	1.4

*) note the software energy cuts in MARS data

VII. SUMMARY

We used MARS and G4beamline codes to simulate pion production in the target, pion and muon collection and transport through the AP2 beamline. At the end of AP2 beamline the observed muon to pion ratio is about 13%, the width of the momentum distribution of pions is $\sigma_p/p_{\rm magic} \approx 1.4\%$, the total number of muons per POT is about 3.9×10^{-7} (for

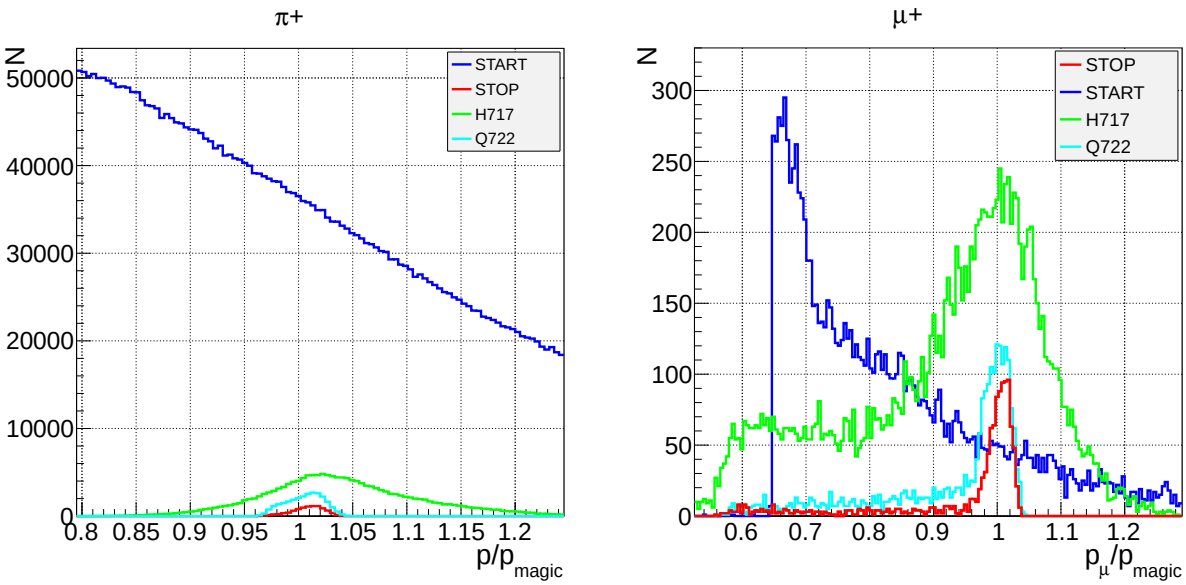

FIG. 6: Momentum distribution of pions (left) or muons (right) in virtual detectors as indicated in the inserts.

TABLE IV: Counting rates of beam particles in virtual detectors per 3.0×10^9 POT. See Figs. 7-15 for details on the momentum cut.

Detector	N_{π^+}	N_{μ^+}	N_{e^+}	N_p
START*)	6.39×10^6	1.17×10^4	1.10×10^5	3.97×10^7
VD_H717	1.62×10^5	1.38×10^4	3.46×10^3	6.98×10^5
VD_Q722	2.64×10^4	2.27×10^3	7.07×10^2	1.14×10^5
STOP	9.16×10^3	1.17×10^3	4.42×10^2	7.40×10^4
VD_Q_703_704	9.11×10^5	4.95×10^4	1.23×10^4	1.83×10^6
VD_Q_705_706	6.12×10^5	3.05×10^4	8.22×10^3	1.23×10^6
VD_Q_709_710	2.93×10^5	2.83×10^4	4.01×10^3	8.11×10^5
VD_Q_714_716	1.94×10^5	2.28×10^4	3.81×10^3	7.72×10^5
VD_Q_727_728	1.84×10^4	2.36×10^3	6.69×10^2	1.08×10^5

*) note the software energy cuts in MARS data

$\sigma_x = \sigma_y =$ 1-mm-wide primary proton beam on target).

[1] D. Still, J. Annala, M. Convery, B. Drendel, S. Johnson, T. Leveling, J. Morgan, and C. Yoshikawa, *g-2 Yield Beam Study Results – Jan 2014*, E989 note 1607 (Fermi National Accelerator Laboratory, 2014).

[2] V. Tishchenko, W. M. Morse, J. F. Ostiguy, J. Morgan, and M. J. Syphers, *MARS and G4beamline simulations: momentum and spin tracking from the production target to the extraction point from the Delivery Ring*, E989 note 1668 (Fermi National Accelerator Laboratory, 2014).

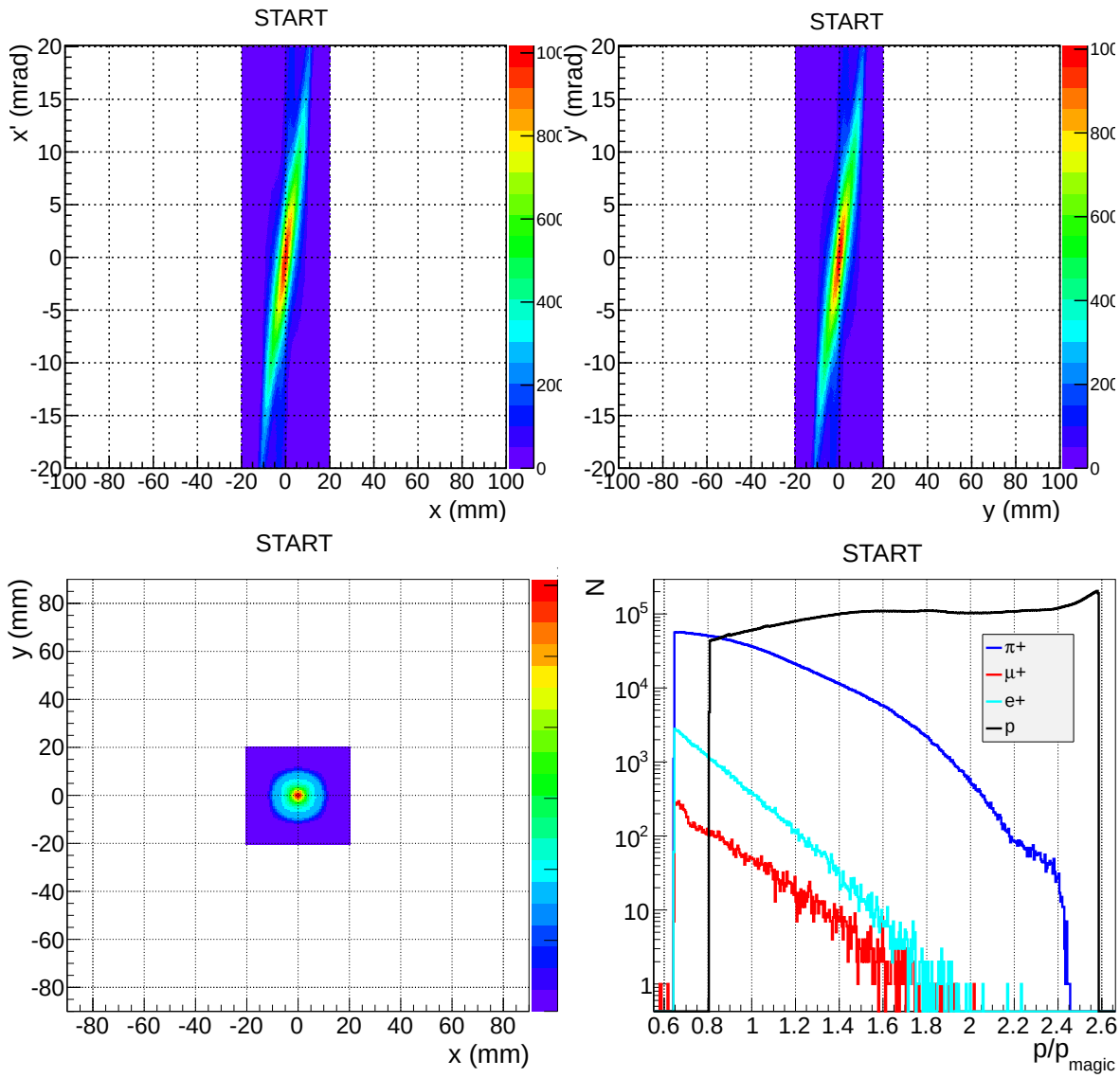

FIG. 7: Horizontal (x-x') and vertical (y-y') phase space distributions of beam particles (top row); coordinate distributions of hits (bottom left) and momentum distributions of beam particles in the virtual detector `START` (bottom right).

[3] V. Tishchenko, W. M. Morse, J. F. Ostiguy, and J. Morgan, *Simulation of Beam Transport Through M2-M3-DR Beamline in* `G4beamline`*: first results*, E989 note 1228 (Fermi National Accelerator Laboratory, 2013).

[4] "The RHIC and ATLAS Computing Facility," `https://www.racf.bnl.gov/`.

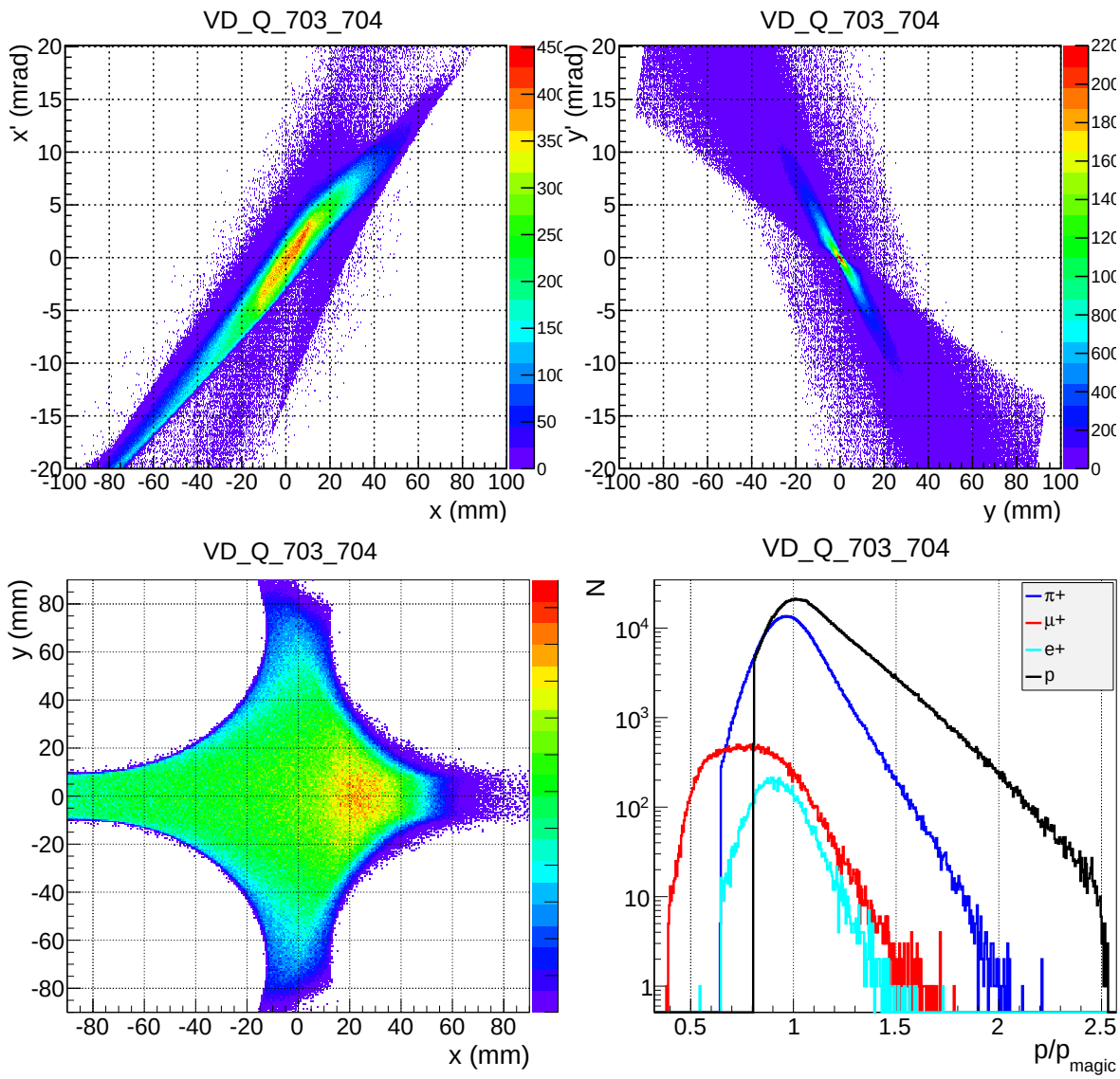

FIG. 8: Horizontal (x-x') and vertical (y-y') phase space distributions of beam particles (top row); coordinate distributions of hits (bottom left) and momentum distributions of beam particles in the virtual detector `VD_Q_703_704` (bottom right).

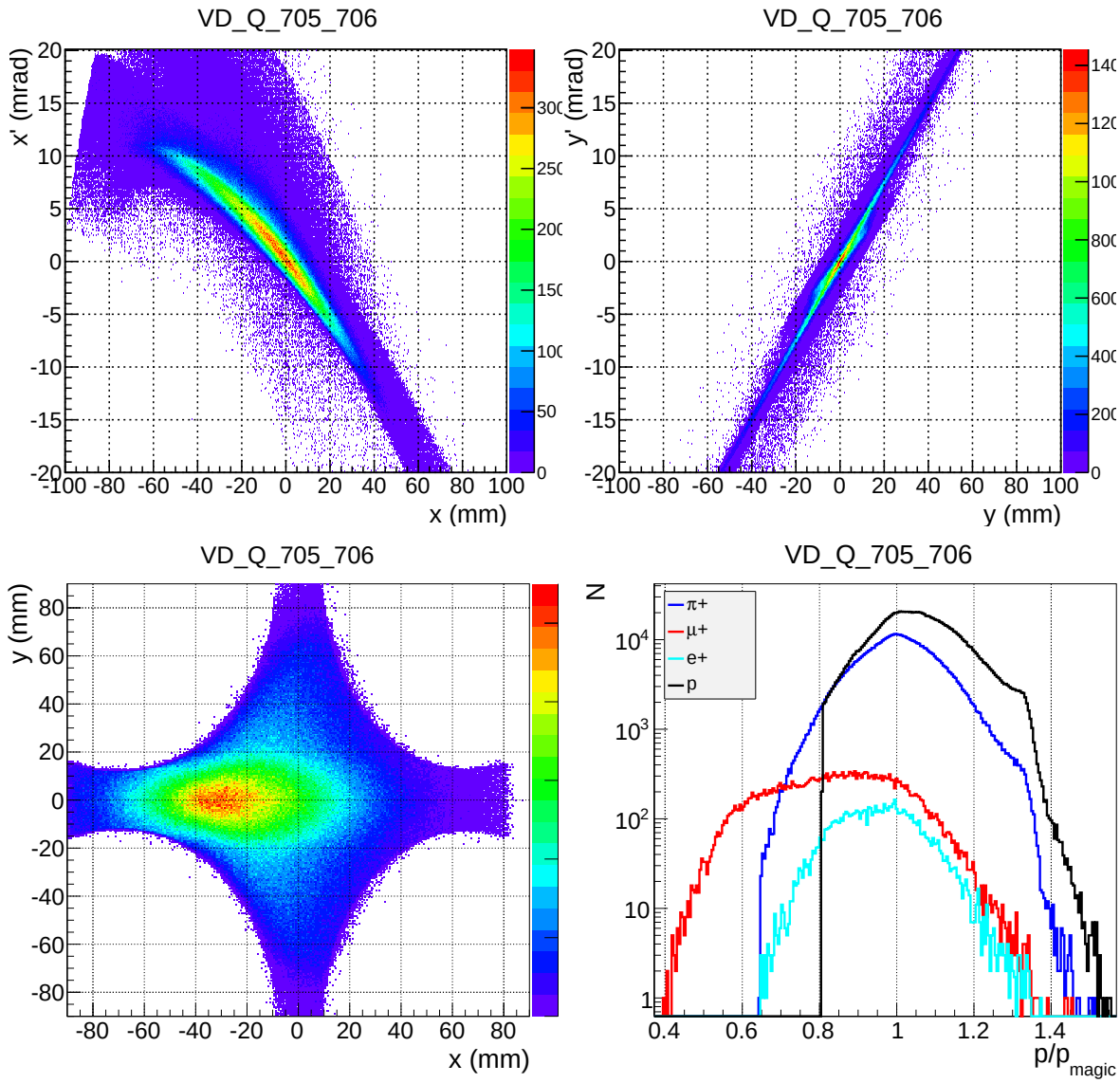

FIG. 9: Horizontal (x-x') and vertical (y-y') phase space distributions of beam particles (top row); coordinate distributions of hits (bottom left) and momentum distributions of beam particles in the virtual detector `VD_Q_705_706` (bottom right).

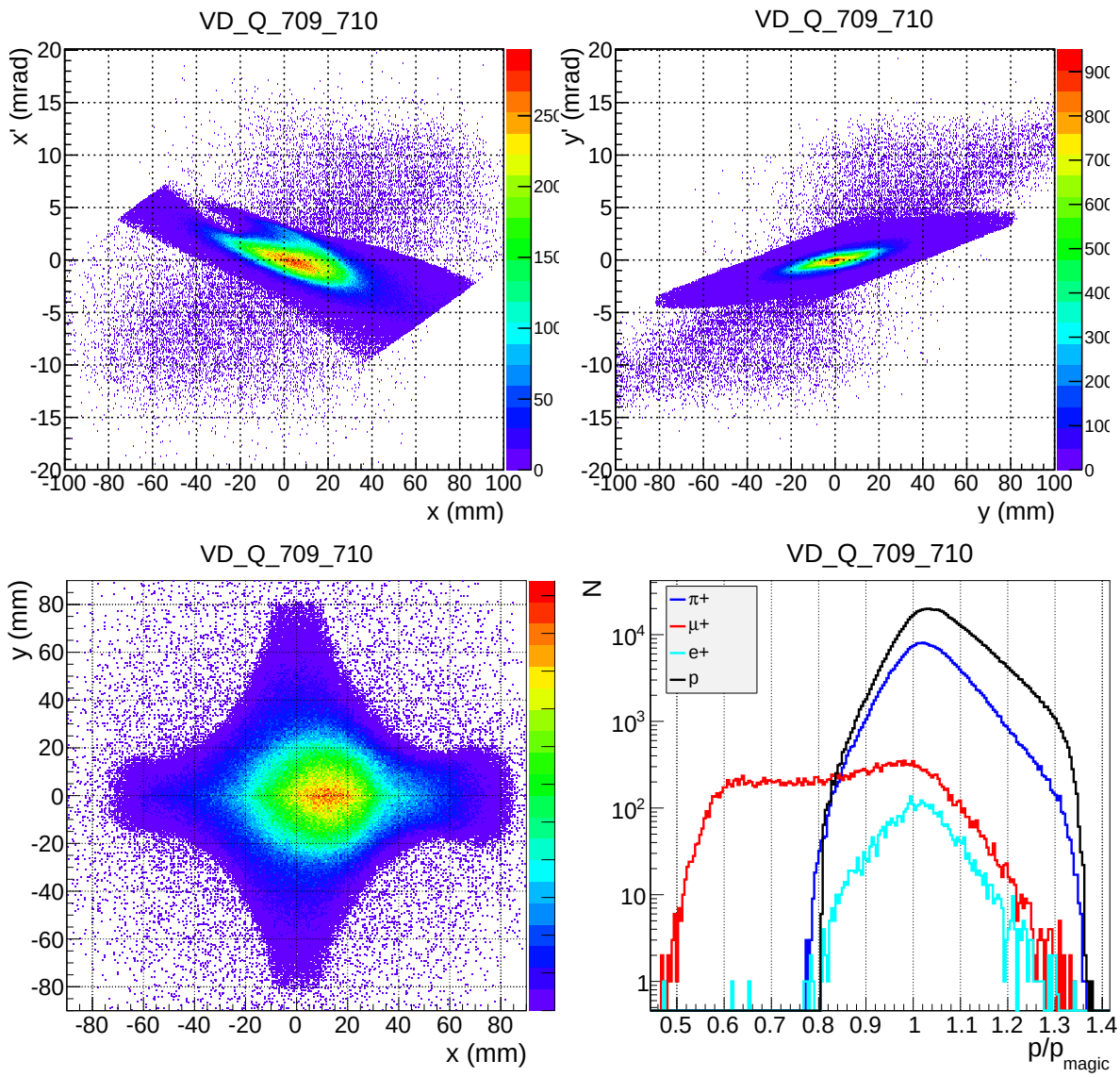

FIG. 10: Horizontal (x-x') and vertical (y-y') phase space distributions of beam particles (top row); coordinate distributions of hits (bottom left) and momentum distributions of beam particles in the virtual detector `VD_Q_709_710` (bottom right).

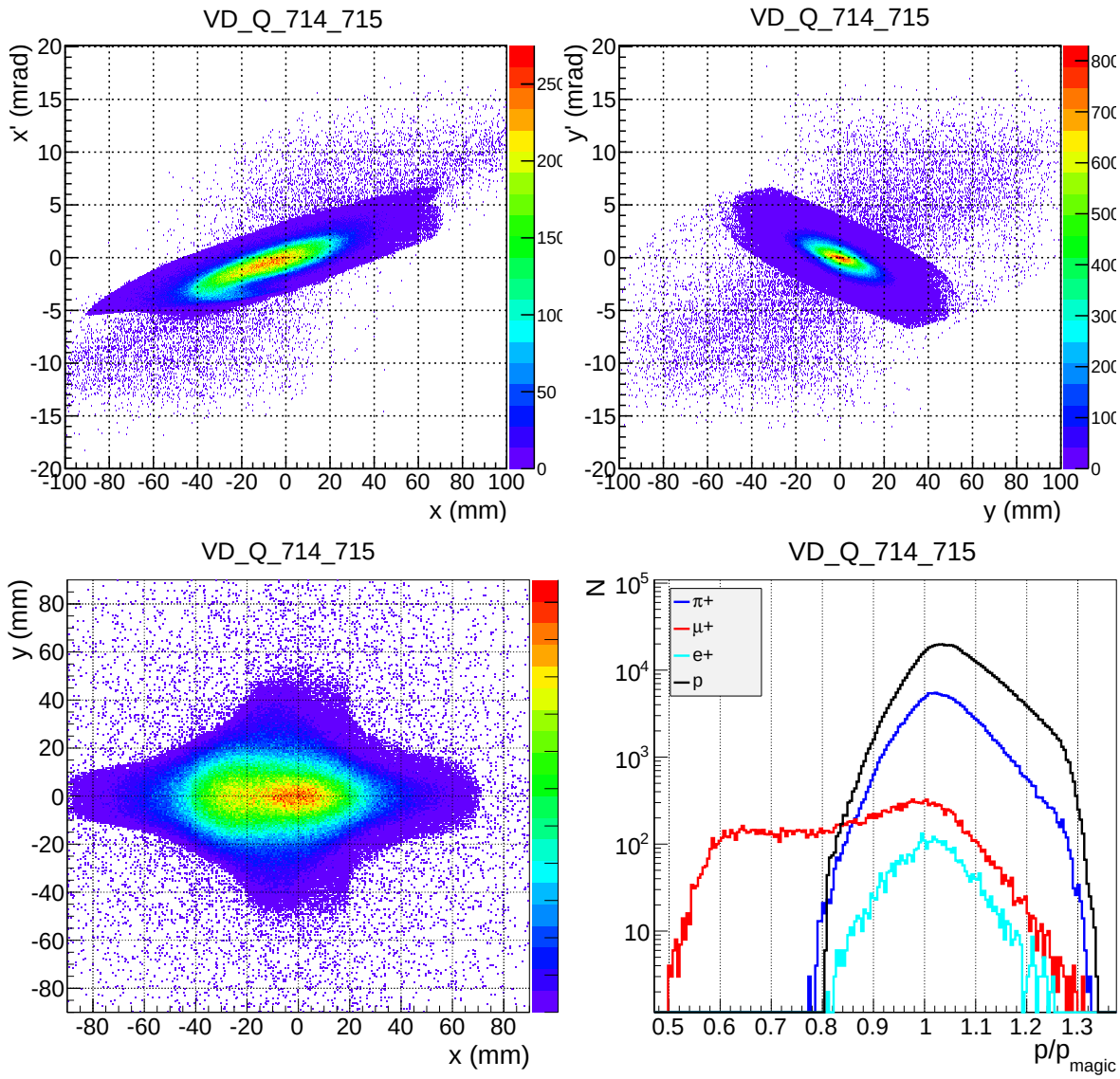

FIG. 11: Horizontal (x-x') and vertical (y-y') phase space distributions of beam particles (top row); coordinate distributions of hits (bottom left) and momentum distributions of beam particles in the virtual detector `VD_Q_714_715` (bottom right).

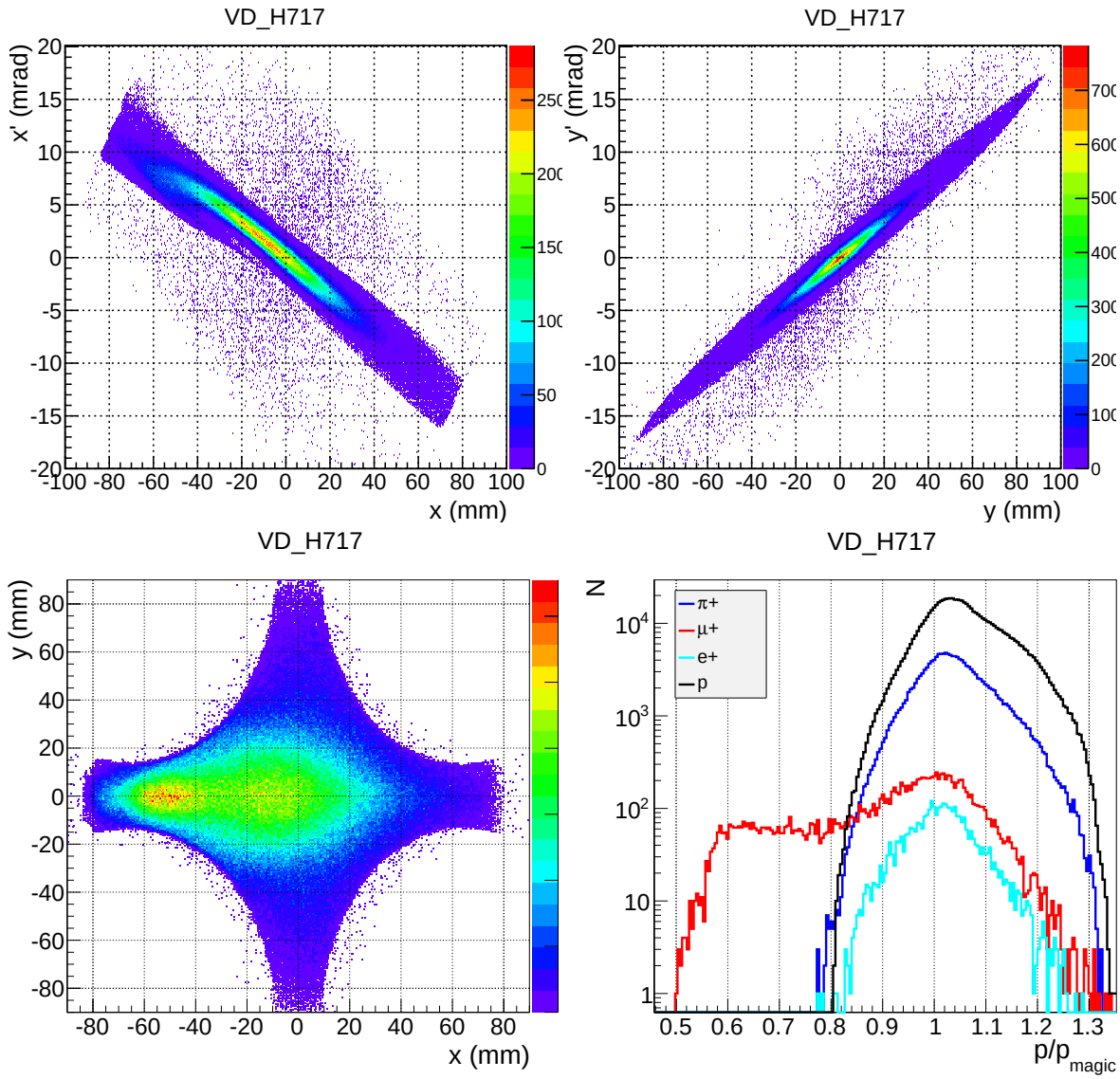

FIG. 12: Horizontal (x-x') and vertical (y-y') phase space distributions of beam particles (top row); coordinate distributions of hits (bottom left) and momentum distributions of beam particles in the virtual detector `VD_H717` (bottom right).

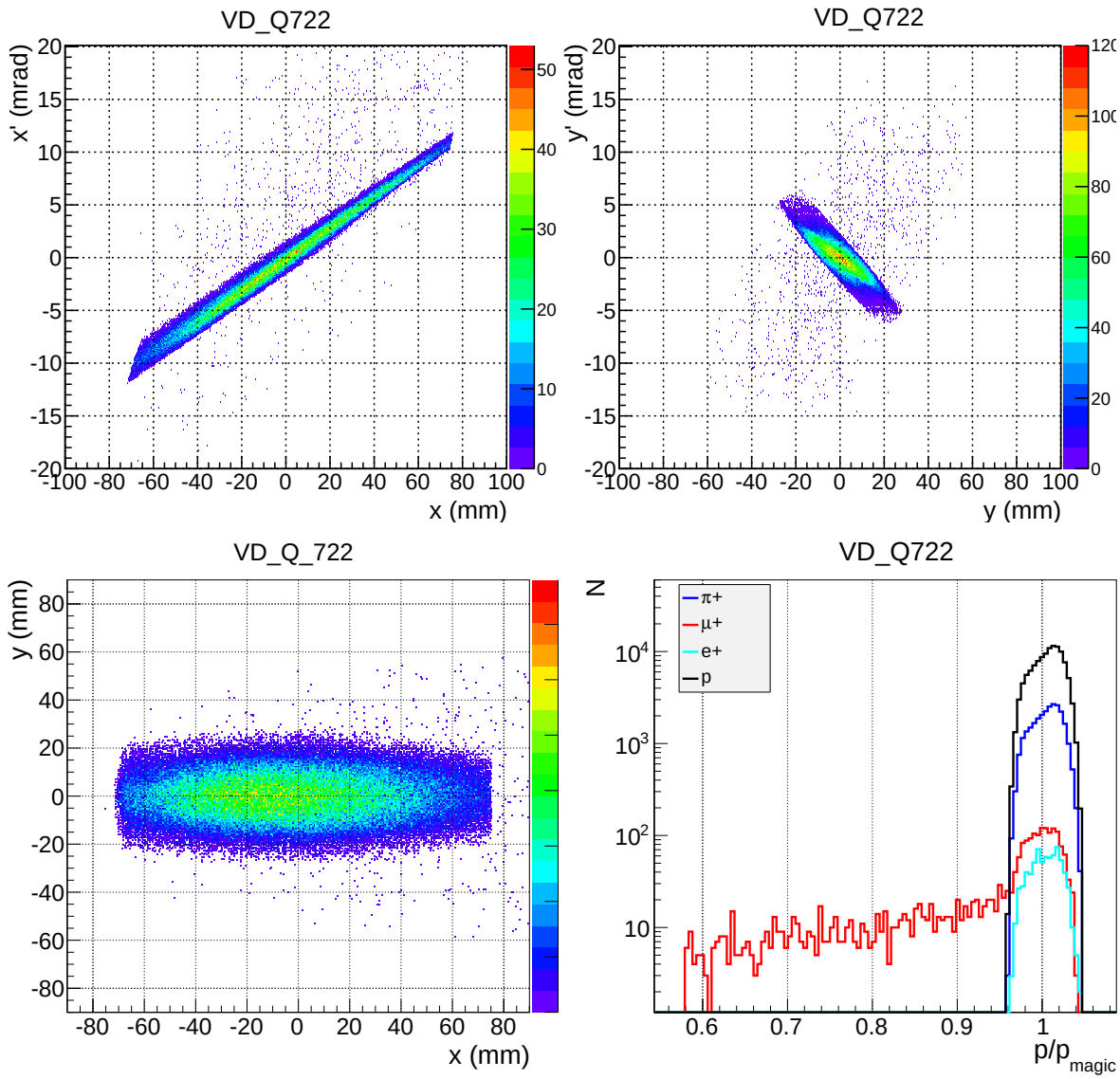

FIG. 13: Horizontal (x-x') and vertical (y-y') phase space distributions of beam particles (top row); coordinate distributions of hits (bottom left) and momentum distributions of beam particles in the virtual detector `VD_Q722` (bottom right).

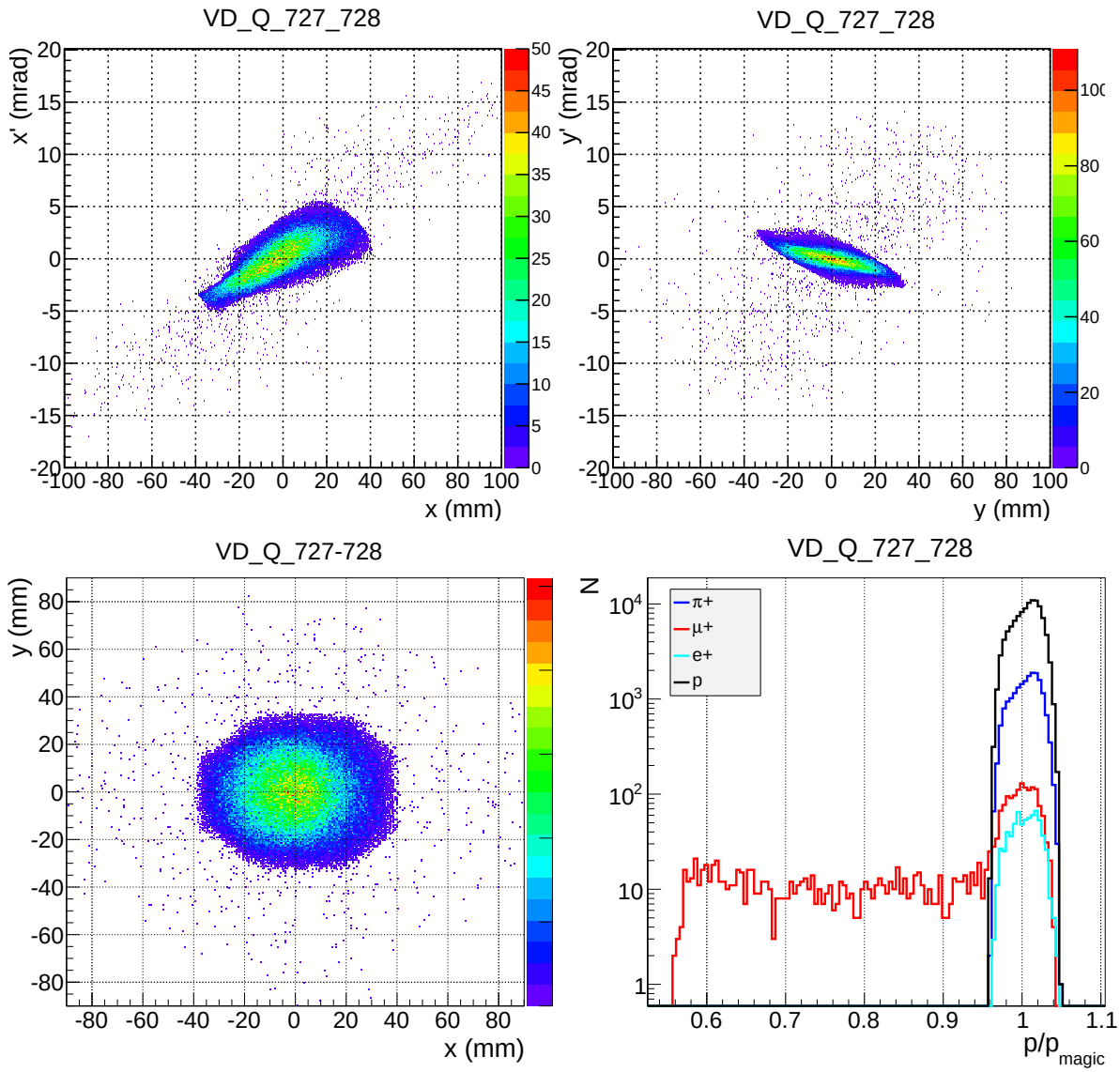

FIG. 14: Horizontal (x-x') and vertical (y-y') phase space distributions of beam particles (top row); coordinate distributions of hits (bottom left) and momentum distributions of beam particles in the virtual detector `VD_Q_727_728` (bottom right).

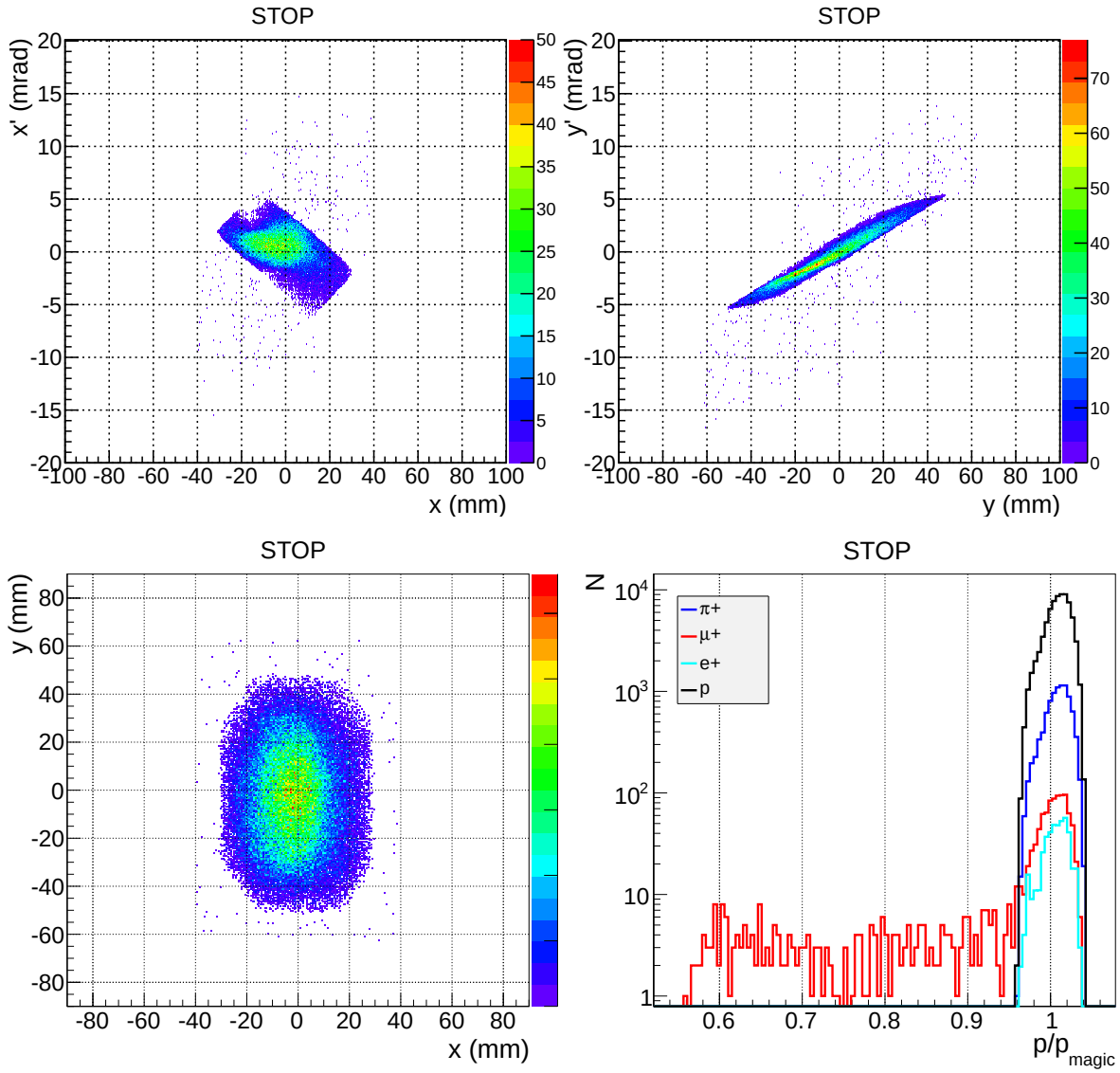

FIG. 15: Horizontal (x-x') and vertical (y-y') phase space distributions of beam particles (top row); coordinate distributions of hits (bottom left) and momentum distributions of beam particles in the virtual detector `STOP` (bottom right).